[23] X. L. Ma, C. Huang, M. B. Pu, C. G. Hu, Q. Feng, and X. G. Luo, "Single-layer circular polarizer using metamaterial and its application in antennas," *Microw. Opt. Tech. Lett.*, vol. 54, no. 7, pp. 1770–1774, Jul. 2012.
[24] D. L. Markovich, A. Andryieuski, M. Zalkovskij, R. Malureanu, and A. V. Lavrinenko, "Metamaterial polarization converter analysis: Limits of performance," *Appl. Phys. B*, 2013, ArXiv: 1209.0095 V1.
[25] E. Arnaud, R. Chantalat, M. Koubeissi, T. Monediere, E. Rodes, and M. Thevenot, "Global design of an EBG antenna and meander-line polarizer for circular polarization," *IEEE Antennas Wireless Propag. Lett.*, vol. 9, pp. 215–218, 2010.
[26] E. Arnaud, R. Chantalat, T. Monediere, and M. Thevenot, "Performance enhancement of self-polarizing metallic EBG antennas," *IEEE Antennas Wireless Propag. Lett.*, vol. 9, pp. 538–541, July 2010.
[27] S. A. Muhammad, R. Sauleau, G. Valerio, L. L. Coq, and H. Legay, "Self-polarizing Fabry-Perot antennas based on polarizing twisting element," *IEEE Trans. Antennas Propag.*, vol. 61, no. 3, pp. 1032–1040, Mar. 2013.
[28] B. Y. Toh, R. Cahill, and V. F. Fusco, "Understanding and measuring circular polarization," *IEEE Trans. Educ.*, vol. 46, no. 3, pp. 313–318, Aug. 2003.

# Composite Right/Left-Handed Ridge Substrate Integrated Waveguide Slot Array Antennas

Qingshan Yang, Xiaowen Zhao, and Yunhua Zhang

***Abstract*—A composite right/left-handed (CRLH) ridge substrate integrated waveguide (RSIW) is proposed and applied to slot array antennas, where the longitudinal slots are etched on the surface of CRLH RSIW, behaving as the radiating elements. Two slot array antennas are designed, fabricated, and measured, one with fixed slot offset, and the other one with varied slot offsets used for achieving low side-lobe level (SLL) of radiation patterns. Compared with the slot array antennas using CRLH rectangular waveguides, the investigated CRLH RSIW ones have the advantages of miniaturized size in transverse direction, relative low cost, low profile, and easy to integrate with other planar circuits. Besides, unlike other proposed planar CRLH leaky wave antennas (LWAs), slots of varied offsets can be adopted on the CRLH RSIW surface to achieve a tapered excitation. Thus the radiation patterns can be optimized for low SLL. In summary, this CRLH RSIW enables a tapered excitation in the beam-steering antenna design while keeps a relative simple structure.**

***Index Terms*—Composite right/left-handed (CRLH), frequency scanning antennas, ridge substrate integrated waveguide (RSIW), slot array antennas.**

## I. Introduction

Composite right/left-handed (CRLH) structures have been paid significant attention over the past decades [1], [2]. They own some unique features not available for traditional microwave structures, e.g., both backward and forward waves, and even infinite-wavelength waves can be supported. These unique properties can be applied to leaky-wave antennas (LWAs) to achieve continuous beam-steering capability from backfire to endfire by varying the frequency, so they can realize a much wider scanning range compared with the traditional LWAs [3]–[14].

To date, numerous CRLH antennas have been reported using microstrip [3]–[6], substrate integrated waveguide (SIW) [7]–[11], and CRLH rectangular waveguide [12]–[14], etc. The microstrip and SIW CRLH structures are usually open to the air and as the CRLH dispersion curves penetrate into the fast-wave region, they are potentially radiative. With the CRLH cells cascaded, a CRLH LWA can be constructed. The power leakage along the LWA with exponential attenuation leads to high side-lobe levels (SLL) in the radiation patterns. With this type of CRLH LWAs, it is difficult to realize a tapered distribution, thereby a low SLL of radiation patterns. Nevertheless, a tapered microstrip CRLH interdigital/stub LWA is realized with minimized SLLs in [6]. The design procedure relies on the co-simulation based on a genetic algorithm, which is rather time-consuming and complex, and only the broadside radiation pattern with low SLL is optimized. Another way of realizing the full-space beam-steering using CRLH rectangular waveguide is reported [13], [14]. A design procedure similar to the traditional waveguide slot array can be employed. This type of CRLH slot array antennas can usually have a better radiation pattern performance compared with the planar CRLH antenna structures. The fabrication of the CRLH waveguides, however, is rather complicated and expensive.

In order to overcome the inherent disadvantages of the already proposed CRLH LWAs, we propose a closed CRLH ridge substrate integrated waveguide (RSIW) and apply it to slot array antennas in this communication. RSIW, similar to traditional ridge waveguide, was originally proposed for the miniaturization of SIW [15]. Compared with the CRLH waveguide adopted in [12]–[14], this CRLH RSIW has the advantages of miniaturized size in transverse direction, relative low cost, low profile, and easy to integrate with other planar circuits. At the same time, this closed planar CRLH structure can keep the energy propagating inside to avoid energy leakage, which is impossible for other microstrip or SIW planar CRLH structures. Based on the CRLH RSIW, slots with varied offsets can be adopted on the surface so as to conveniently realize a tapered excitation distribution, as done in traditional rectangular waveguide slot antenna design. Usually it is difficult to achieve for the planar CRLH LWAs. Here, the taper design for slot excitation is different from that used in [14], as shown in the beginning of Section V. Another slot array antenna based on the folded substrate integrated waveguide (FSIW) was proposed in [16], where the rotated radiating slot is confined to the CRLH FSIW cell, which results in rather low radiation efficiency. The antenna is constructed directly by cascading the radiative CRLH FSIW cells as usual LWAs do, so it does not have a tapered excitation distribution.

This communication is organized as follows. The geometry of the closed CRLH RSIW is illustrated in Section II, where the dispersion and loss analysis of the CRLH RSIW are also discussed. Section III investigates the slot type and advantages of this CRLH RSIW slot array antenna. In Sections IV and V, two slot array antennas are designed, fabricated, and measured. Finally, some conclusions are drawn in Section VI.

## II. CRLH RSIW

A closed CRLH RSIW for the slot array antenna is proposed in this section. The prototype is built on a two-layer substrate of Rogers RT/Duroid 6002 with dielectric constant $\varepsilon_r = 2.94$, loss tangent

Manuscript received April 22, 2013; revised June 27, 2013; accepted January 14, 2014. Date of publication January 27, 2014; date of current version April 03, 2014.

Q. Yang and X. Zhao are with the University of Chinese Academy of Sciences, Beijing, 100049, China and also with the Key Laboratory of Microwave Remote Sensing, Center for Space Science and Applied Research, Chinese Academy of Sciences, Beijing, 100190, China (e-mail: flyangster@gmail.com; xiaowenzhao923@gmail.com).

Y. Zhang is with the Key Laboratory of Microwave Remote Sensing, Center for Space Science and Applied Research, Chinese Academy of Sciences, Beijing, 100190, China (e-mail: zhangyunhua@mirslab.cn).

Color versions of one or more of the figures in this communication are available online at http://ieeexplore.ieee.org.

Digital Object Identifier 10.1109/TAP.2014.2302834

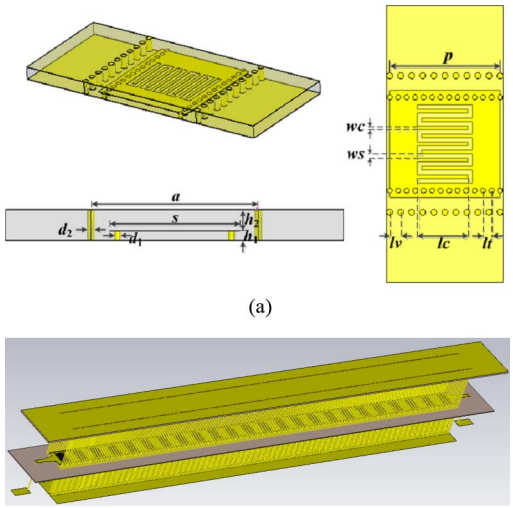


(a)

(b)

Fig. 1. The layout of the proposed CRLH RSIW (a) unit cell, (b) overall prototype with 24 unit cells.

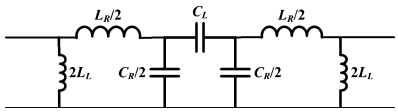


Fig. 2. The equivalent circuit for the CRLH RSIW unit cell.

$\tan\delta = 0.0012$. The multi-layer printed-circuit board (PCB) process is adopted to fabricate the CRLH RSIW.

### A. Configuration

Fig. 1(a) depicts the configuration of the CRLH RSIW unit cell. The thicknesses of the two layers are $h_1 = 0.254$ mm, $h_2 = 0.508$ mm, respectively. A bonding film with dielectric constant of 2.8 and loss tangent of 0.01 is used to stick the two substrates together. In the fabrication, vertical metal walls of the RSIW are implemented using metallized vias with the diameters $d_1 = 0.3$ mm and $d_2 = 0.35$ mm, respectively. A RSIW based CRLH transmission line can be constructed by periodically cascading the unit cell. Two sections of tapered microstrip line which also serve as the match network to 50 $\Omega$, are designed to connect to the ridge surface of the CRLH RSIW at the two ends, and the top metal plate of the upper substrate serves as the corresponding ground, as shown in Fig. 1(b). The tapered feeding line sandwiched in the substrates can be switched to the bottom plate of the lower substrate through a metal via so as to connect to the SMA conveniently [17].

### B. Dispersion and Loss Analysis

The CRLH property is obtained by etching interdigital slots on the ridge surface of the RSIW. The slots behaving as the series capacitors together with the shunt inductors provided by the metal vias, construct the left-handed (LH) condition to support the backward-wave. The inherent distributed series inductors and shunt capacitors provide the right-handed (RH) condition. Fig. 2 presents the equivalent circuit model for the CRLH RSIW unit cell. A balanced condition can be achieved if the series resonant frequency equals to the shunt resonant frequency, i.e.,

$$\omega_{se} = \omega_{sh} \tag{1}$$

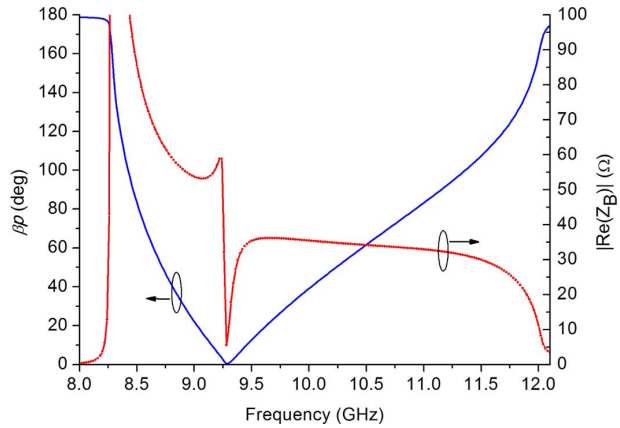


Fig. 3. The dispersion and Bloch impedance for the CRLH RSIW cell.

TABLE I
DIMENSIONS FOR THE CRLH RSIW CELL

| Parameter: | *a* | *s* | *lc* | *wc* | *ws* | *p* | *lv* | *lt* |
|---|---|---|---|---|---|---|---|---|
| Unit: mm | 8.05 | 6.3 | 3 | 0.21 | 0.26 | 6.5 | 0.65 | 0.5 |

where

$$\omega_{se} = \frac{1}{\sqrt{L_R C_L}} \quad \omega_{sh} = \frac{1}{\sqrt{L_L C_R}}. \tag{2}$$

Under this balanced condition, the propagation constant $\beta$ can be expressed as

$$\beta = \beta^{RH} + \beta^{LH} = \frac{\omega}{p}\sqrt{L_R C_R} - \frac{1}{\omega p \sqrt{L_L C_L}} \tag{3}$$

where $p$ is the length of the unit cell. The propagation constant $\beta$ exhibits zero at the following transition frequency

$$\omega_0 = \frac{1}{\sqrt[4]{L_R C_R L_L C_L}} = \omega_{se} = \omega_{sh}. \tag{4}$$

Bloch impedance is used to characterize the impedance of a unit cell in a periodic transmission line. It provides a reference for the impedance matching of the periodic transmission structure. For a CRLH unit cell, the Bloch impedance $Z_B$ is expressed as [1]

$$Z_B = Z_L \sqrt{\frac{\left(\frac{\omega}{\omega_{se}}\right)^2 - 1}{\left(\frac{\omega}{\omega_{sh}}\right)^2 - 1} - \left\{\frac{\omega_L}{2\omega}\left[\left(\frac{\omega}{\omega_{se}}\right)^2 - 1\right]\right\}^2} \tag{5}$$

where

$$Z_L = \sqrt{\frac{L_L}{C_L}} \quad \omega_L = \frac{1}{\sqrt{L_L C_L}}. \tag{6}$$

It is seen that $\omega_{se}$ and $\omega_{sh}$ correspond to a zero and a pole, respectively. The zero and pole always exist unless the balanced condition of (1) is strictly satisfied.

In this communication, a CRLH RSIW operated at X-band is designed. The other dimensions for the CRLH RSIW unit cell are listed in Table I. Fig. 3 depicts the corresponding dispersion and Bloch impedance for the CRLH RSIW cell extracted from the simulated S-parameters using Ansoft HFSS [18]. We can see from Fig. 3 that the CRLH cell is balanced at 9.3 GHz approximately. Below this frequency, the LH region appears which supports the backward-wave propagation, and just above the transition frequency, the RH region

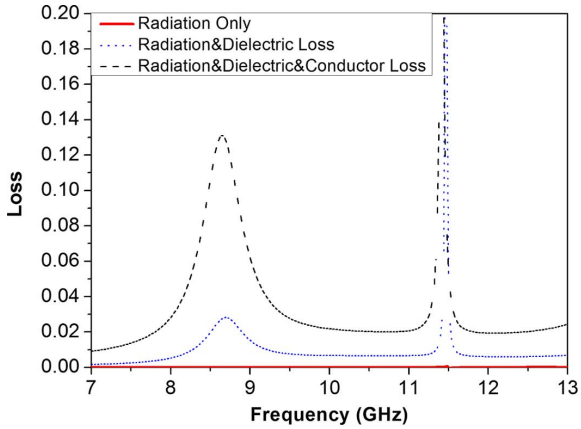


Fig. 4. The curves of loss versus frequency of the CRLH RSIW cell.

Fig. 5. The fabricated CRLH RSIW with 24 unit cells, acting as the feeding structure for the slot array antennas.

supporting the forward-wave appears. A null is exhibited for the propagation constant $\beta$ at 9.3 GHz. A rapid change corresponding to a zero and a pole is observed near the transition frequency from the Bloch impedance curve, which is consistent with the results of (5). The Bloch impedance curve presents a flat behavior in the RH region while presents noticeable variation in the LH region, which means the balanced condition is not so perfect. A more accurate but time-consuming eigen-mode simulation may be applied to improve the balanced condition. The average Bloch impedance from 8.5 GHz to 12 GHz is around 38 $\Omega$, so a taper line matching network is adopted to transform 38 $\Omega$ to 50 $\Omega$.

Fig. 4 shows the loss analysis for the CRLH RSIW cell calculated by

$$Loss = 1 - S_{11}S_{11}^{*} - S_{21}S_{21}^{*}. \tag{7}$$

The loss curves clearly show that the radiation loss is so small that it can be even neglected. It is to say the non-radiation property of this closed CRLH RSIW structure is validated. The abrupt high loss around 11.5 GHz is due to the strong resonance.

### C. S-Parameters

A CRLH RSIW with 24 unit cells is fabricated as shown in Fig. 5. Fig. 6 gives the simulated $S$-parameters using CST Microwave Studio, and the measured $S$-parameters by Agilent PNA-X Network Analyzer, they agree very well with each other. The increased conductor loss and the reflection of SMA connectors are the main reasons for the discrepancy between the simulated and measured magnitudes of $S_{21}$. The decrease around 11.5 GHz is consistent with the loss analysis in Fig. 4. A frequency bandwidth of $S_{11} < -10$ dB is achieved from 8 GHz to more than 12 GHz except for a narrow frequency band around the transition frequency. This is mainly caused by the mismatch of Bloch impedance to 50 $\Omega$ near the transition frequency as shown in Fig. 3.

Based on the fabricated CRLH RSIW, slots can be etched on the top surface, which behave as the radiating elements.

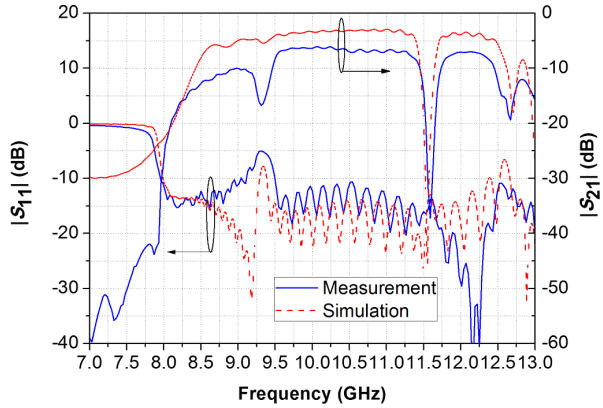


Fig. 6. The simulated and measured $S$-parameters for the 24-unit-cell CRLH RSIW.

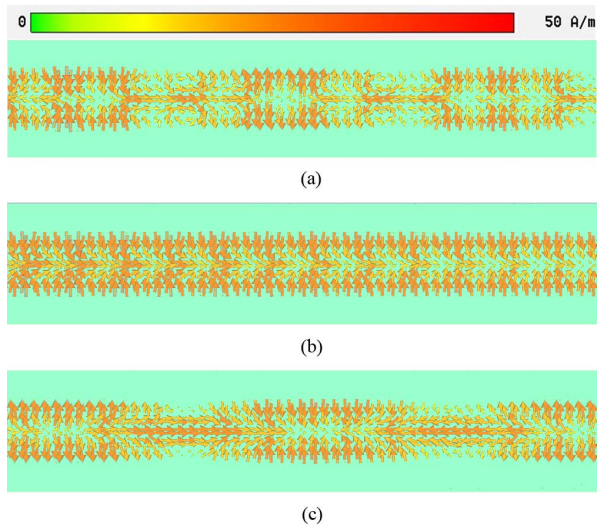


Fig. 7. The surface current distributions on the top face of the CRLH RSIW at different frequencies. (a) 8.8 GHz, LH region, (b) 9.3 GHz, transition frequency, (c) 10.0 GHz, RH region.

## III. CRLH Slot Array Antenna

In traditional rectangular waveguide slot array antennas, three types of radiating slot are usually adopted on the broad face of the waveguide, i.e., transverse series slot, longitudinal shunt slot and rotated series slot. All these slots are excited by the corresponding surface current perpendicular to the long edge of the slot. The surface current distribution on the top face of the CRLH RSIW is simulated using CST Microwave Studio, as shown in Fig. 7, which is very similar to that on traditional rectangular waveguide, even when the propagation constant $\beta$ is negative or zero. Thus the three types of slot can still be applied to this CRLH RSIW slot array antenna. Besides, in order to achieve the best radiation efficiency, the slot should cut the surface current perpendicularly where the largest current density is distributed. Thus the longitudinal slot with offset would be the best choice according to the surface current distribution in Fig. 7. In our design, all the longitudinal slots are arranged on the same side of the CRLH RSIW center line. In this way, the CRLH slot array antenna can realize a full space scanning range including backward and broadside radiations, that is difficult to realize for traditional waveguide ones [14].

Two slot array antennas are designed, fabricated, and measured, one with a fixed slot offset is for demonstrating the continuous beam-steering capability from backward to forward, and the other

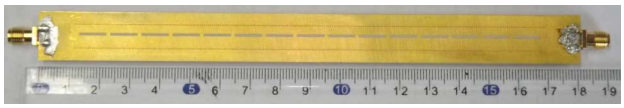

Fig. 8. The fabricated CRLH RSIW 15-slot-array antenna with fixed slot offset.

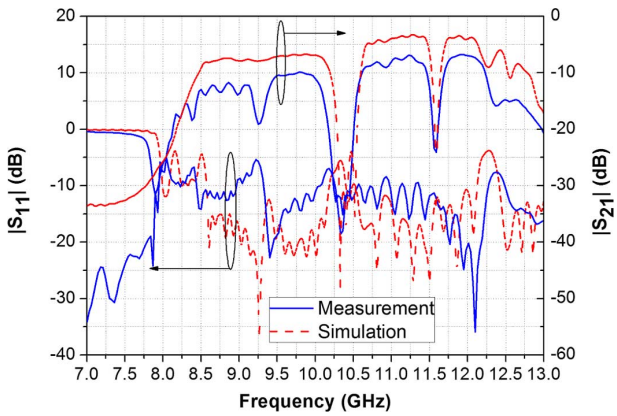


Fig. 9. The simulated and measured $S$-parameters for the 15-slot-array antenna with fixed slot offset.

one with varied slot offsets is for demonstrating the optimized SLL performance.

## IV. CRLH RSIW Slot Array Antenna With Fixed Slot Offset

Fig. 8 shows the fabricated slot array antenna based on the 24-unit-cell CRLH RSIW. In this design, 15 equally spaced longitudinal slots are etched on the broad face of the CRLH RSIW with the same length of $l_{slot} = 9$ mm, and the width of $w_{slot} = 0.8$ mm. The spacing $d$ between the neighboring slots is 10.3 mm, all the slot offsets are designed to be the same with $\delta = 0.7$ mm. For this array, the power radiated from the slots experiences an exponential attenuation.

Fig. 9 presents both the simulated and the measured $S$-parameters of this CRLH slot array antenna. Compared with the $S$-parameters of the closed CRLH RSIW presented in Fig. 6, the magnitude of $S_{21}$ from 8.6 GHz to 10.3 GHz decreases because the radiation happens, and the more the $S_{21}$ magnitude decreases, the better the radiation efficiency can be realized. But in the frequency region from 10.5 GHz to 13 GHz, the $S_{21}$ magnitude is about the same as that in Fig. 6, which means low radiation efficiency and it is not suitable for antenna application. Thus the frequency band of interest is focused on the region from 8.6 GHz to 10.3 GHz. Another difference should be noticed is that a new strong resonance appears near 10.4 GHz. We think it is caused by the resonance of the slots. The manufacturing error should be the reason for resulting the discrepancy between the simulated and measured $S_{11}$ magnitudes in the LH region.

Fig. 10 shows the normalized H-plane radiation patterns measured at different frequencies. The full space continuous beam-steering capability of this CRLH RSIW slot array antenna is clearly demonstrated. As a result of an exponential distribution of the slot excitation, the SLL is above $-10$ dB for the radiation patterns presented in Fig. 10.

The measured main beam angles for the radiation patterns at different frequencies are plotted in Fig. 11. A scanning range from $-46^{\circ}$ to $+40^{\circ}$ is obtained when the frequency varies from 8.6 GHz to 10.3 GHz with a relative bandwidth of 18.3% (1.7 GHz bandwidth centered at 9.3 GHz). Fig. 12 gives the simulated and measured antenna gains as well as the simulated radiation efficiencies. The largest gain of 11.5 dBi is achieved at 10.0 GHz. A dip in gain near the transition frequency is mainly due to the mismatch of the Bloch

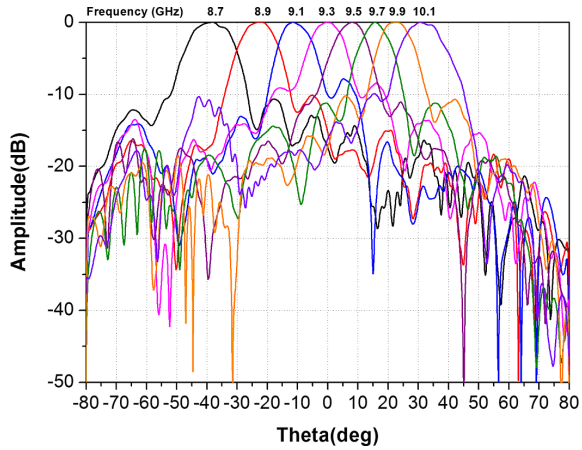


Fig. 10. The measured radiation patterns at different frequencies for the 15-slot-array antenna with fixed slot offset.

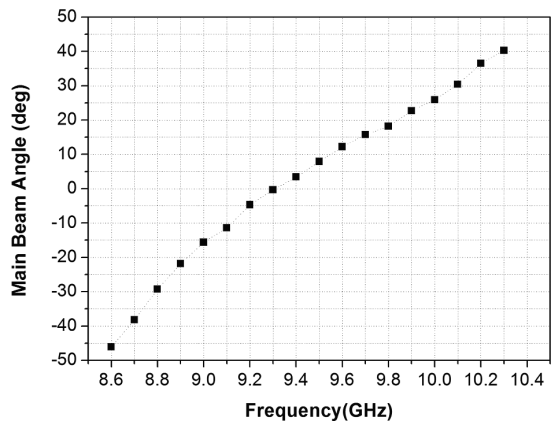


Fig. 11. The measured main beam angles at different frequencies for the CRLH RSIW 15-slot array antenna with fixed slot offset.

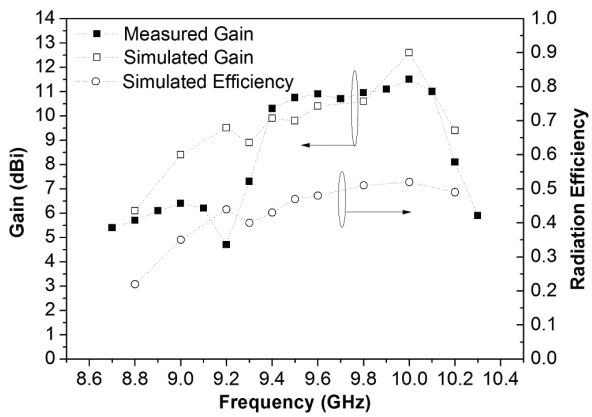


Fig. 12. The gain and the simulated radiation efficiency for the 15-slot-array antenna with fixed slot offset.

impedance to 50 Ω. As observed the $S_{11}$ magnitude increases and thus most of the energy is reflected back to the source rather than radiated along the antenna. Discrepancies between the simulated and measured gains are exhibited in the LH region. We think the manufacturing error and the soldering lead to a larger measured $S_{11}$ magnitude than the simulated one, as shown in Fig. 9. The radiation efficiency is less than 40% when the frequency is below 9.0 GHz. It is mainly caused by both the conductor and dielectric losses in this

TABLE II
SLOT EXCITATION AND OFFSETS FOR THE CRLH RSIW 15-SLOT-ARRAY ANTENNA DESIGN.

| Slot No. | 1 | 2 | 3 | 4 | 5 | 6 | 7 | 8 | 9 | 10 | 11 | 12 | 13 | 14 | 15 |
|---|---|---|---|---|---|---|---|---|---|---|---|---|---|---|---|
| $A_n$ | 0.52 | 0.56 | 0.64 | 0.73 | 0.83 | 0.92 | 0.98 | 1 | 0.98 | 0.92 | 0.83 | 0.73 | 0.64 | 0.56 | 0.52 |
| $\delta$ (mm) | 0.25 | 0.29 | 0.33 | 0.39 | 0.46 | 0.53 | 0.6 | 0.65 | 0.71 | 0.76 | 0.78 | 0.78 | 0.76 | 0.71 | 0.71 |

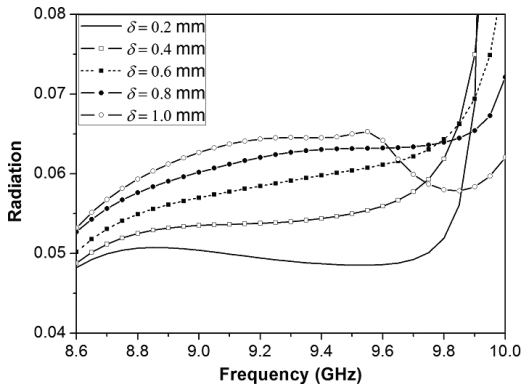


Fig. 13. The single slot radiation versus different offsets.

frequency region. A bonding film with a low dielectric loss tangent is helpful for decreasing the dielectric loss while increasing the radiation efficiency. The impedance mismatch in the LH region also causes the low radiation efficiency.

## V. CRLH RSIW SLOT ARRAY ANTENNA WITH VARIED SLOT OFFSETS

In Section IV, the CRLH RSIW slot array antenna with fixed slot offset is investigated. As we know in the CRLH RSIW slot array antenna, the radiation comes from the energy leakage of the slots. Thus the slot parameters (e.g., slot widths and offsets) determine the radiation strength. By controlling the slot parameters, a tapered excitation distribution can be designed to achieve a low SLL performance. In the tapered distribution design in [14], the admittance properties of the longitudinal slot are analyzed at two different frequencies located in the LH region and RH region, respectively. The final slot lengths and offsets are determined by just arithmetically averaging the obtained dimensions at the two frequencies. In this design, more emphasis is on the analysis of the single slot radiation versus varied slot offsets at the transition frequency since the guided wavelength is infinite and the CRLH RSIW structure is uniform.

For a longitudinal slot placed on the surface of a CRLH RSIW, the slot radiation can be calculated by (7) assuming that the dielectric and conductor are lossless. By varying the slot offset, a group of radiation powers are calculated and plotted in Fig. 13. The slot length $l_{slot}$ and width $w_{slot}$ are 9 mm and 0.8 mm, respectively. It is seen that the bigger the slot offset, the larger the amount of radiation in the frequency band of interest. This radiation property can be applied to achieve a desired excitation distribution such as Taylor distribution. A wider slot is helpful for enhancing the radiation and improve the radiation efficiency, so, a similar excitation distribution can also be realized by varying the slot widths, which is not discussed here.

The design of a 15-slot-array antenna with varied slot offsets is based on the plots of Fig. 13. The transition frequency of 9.3 GHz is chosen as the design frequency. A Taylor pattern with $-20$ dB SLL is targeted. The slot excitation $A_n$ and the corresponding offsets $\delta$ are given in Table II. The 15 slots are all lying on the same side of the center line,

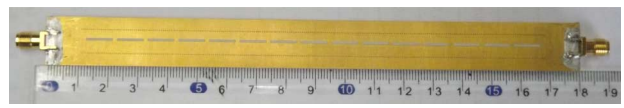

Fig. 14. The fabricated CRLH RSIW 15-slot-array antenna with varied slot offsets.

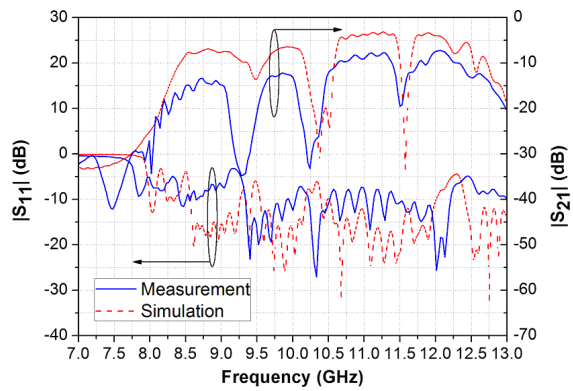


Fig. 15. The simulated and measured $S$-parameters for the 15-slot-array antenna with varied slot offsets.

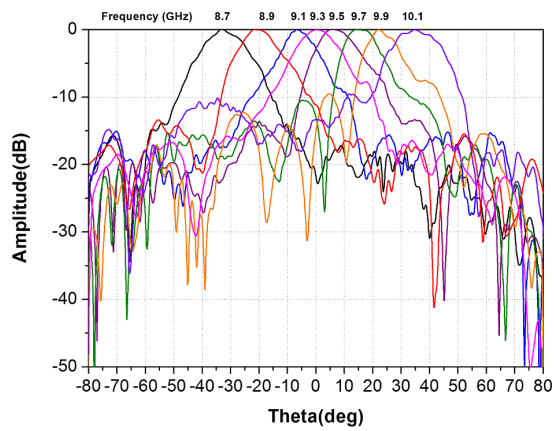


Fig. 16. The measured radiation patterns at different frequencies for the 15-slot-array antenna with varied slot offsets.

uniformly spaced with a distance $d = 10.3$ mm. The slots are numbered beginning from the closest one to the feeding port. Fig. 14 gives the photography of the fabricated CRLH RSIW 15-slot-array antenna with varied slot offsets. The simulated and measured S-parameters are presented in Fig. 15. By comparing the S-parameters of Fig. 15 with that of Fig. 9, we can see that the $S_{21}$ magnitude has been deteriorated near the transition frequency. This is because the balanced condition of the CRLH structure is slightly deteriorated by the slots of different offsets. The radiated frequency band of interest is from 8.6 GHz to 10.3 GHz, which is as same as that of the slot array with fixed slot offset.

The normalized radiation patterns at the same frequencies as Fig. 10 are measured and plotted in Fig. 16. The requirement of

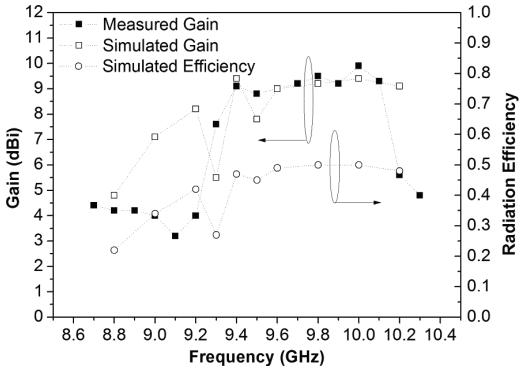


Fig. 17. The gain and the simulated radiation efficiency for the 15-slot-array antenna with varied slot offsets.

$-20$ dB SLL is not strictly met since the mutual coupling between neighboring slots is not considered in the design procedure currently. The SLLs of the H-plane radiation patterns at 8.7 GHz, 8.9 GHz and 9.1 GHz are about $-15$ dB, i.e., $-5$ dB lower than that in Fig. 10. The SLL of the broadside pattern is better than $-15$ dB in Fig. 16, while in Fig. 10, it is above $-10$ dB. The SLLs of the radiation patterns in the RH region in Fig. 16 is only about $-10$ dB. We think this is due to the power is dissipated by the dielectric and conductor losses of the CRLH RSIW so that the slots near the matched load cannot obtain the expected excitation amplitude. Nevertheless, the SLL is still better than that in Fig. 10.

Fig. 17 shows the antenna gain and simulated radiation efficiency of this CRLH RSIW slot array , the maximum gain of 9.9 dBi is obtained at 10.0 GHz. Good agreements between the simulated and measured gains are shown in the RH region; while in the LH region, discrepancies are observed due to the same reason as that of the fixed offset case.

## VI. Conclusions

This communication has investigated the slot array antennas based on a CRLH RSIW structure. A closed CRLH RSIW for slot array antenna is first developed with the dispersion and loss characteristics analyzed and discussed, then two slot array antennas with different radiation characteristics are investigated. Experiment results confirm their full space beam-steering performance from the backward $(-46^\circ)$ to the forward $(+40^\circ)$ as the frequency sweeps from 8.6 GHz to 10.3 GHz. Optimization for achieving low SLL of radiation patterns is carried out by varying the slot offsets. The radiation patterns for the slot array antenna with varied slot offsets are compared with that of the slot array antenna with fixed slot offset and the SLL improvements are clearly demonstrated. In fact, we can realize low SLL through other way, e.g., by varying the slot widths. We want to point out that rotated slots can also be adopted on the broad surface of the CRLH RSIW for dual-polarization antennas. In summary, the CRLH RSIW slot array antennas have the advantages of miniaturized size in transverse direction, low profile, and easy to realize a tapered excitation, which are difficult to achieve simultaneously for other planar CRLH LWAs. The proposed antennas is expected to have applications in the future in radar systems which require very wide range of beam-steering.

## Acknowledgment

The authors would like to thank Prof. H. Wang, and Dr. M. Yi (Center for Space Science and Applied Research, Chinese Academy of Sciences) for their kind help on antenna measurements.

## References

[1] C. Caloz and T. Itoh, *Electromagnetic Metamaterials: Transmission Line Theory and Microwave Applications: the Engineering Approach*. New York, NY, USA: Wiley-IEEE Press, 2006.

[2] G. Eleftheriades and K. Balmain, *Negative-Refraction Metamaterials: Fundamental Principles and Applications*. New York, NY, USA: Wiley-IEEE Press, 2005.

[3] L. Lei, C. Caloz, and T. Itoh, "Dominant mode leaky-wave antenna with backfire-to-endfire scanning capability," *Electron. Lett.*, vol. 38, pp. 1414–1416, 2002.

[4] F. P. Casares-Miranda, C. Camacho-Penalosa, and C. Caloz, "High-gain active composite right/left-handed leaky-wave antenna," *IEEE Trans. Antennas Propag*, vol. 54, pp. 2292–2300, 2006.

[5] S. Paulotto, P. Baccarelli, F. Frezza, and D. R. Jackson, "Full-Wave Modal Dispersion Analysis and Broadside Optimization for a Class of Microstrip CRLH Leaky-Wave Antennas," *IEEE Trans. Microw. Theory Tech.*, vol. 56, pp. 2826–2837, 2008.

[6] R. Siragusa, E. Perret, P. Lemaitre-Auger, H. Van Nguyen, S. Tedjini, and C. Caloz, "A Tapered CRLH Interdigital/Stub Leaky-Wave Antenna With Minimized Sidelobe Levels," *IEEE Antennas Wireless Propag. Lett.*, vol. 11, pp. 1214–1217, 2012.

[7] Y. Weitsch and T. F. Eibert, "Continuous beam-steering leaky-wave antenna based on substrate integrated waveguide," in *Proc. 2nd Eur. Conf. on Antennas and Propagation, EuCAP*, 2007, pp. 1–5.

[8] D. Yuandan and T. Itoh, "Composite right/left-handed substrate integrated waveguide and half mode substrate integrated waveguide leaky-wave structures," *IEEE Trans. Antennas Propag.*, vol. 59, pp. 767–775, 2011.

[9] D. Yuandan and T. Itoh, "Substrate integrated composite right-/left-handed leaky-wave structure for polarization-flexible antenna application," *IEEE Trans. Antennas Propag.*, vol. 60, pp. 760–771, 2012.

[10] Q. Yang, Y. Zhang, and X. Zhang, "X-band composite right/left-handed leaky wave antenna with large beam scanning-range/bandwidth ratio," *Electron. Lett.*, vol. 48, pp. 746–747, 2012.

[11] Q. Yang, X. Zhang, and Y. Zhang, "A shunt-capacitance-aided composite right/left-handed leaky wave antenna with large scanning-range /bandwidth ratio," in *PIERS Proc.*, Moscow, Russia, 2012, pp. 649–652.

[12] T. Ikeda, K. Sakakibara, T. Matsui, N. Kikuma, and H. Hirayama, "Beam-scanning performance of leaky-wave slot-array antenna on variable stub-loaded left-handed waveguide," *IEEE Trans. Antennas Propag.*, vol. 56, pp. 3611–3618, 2008.

[13] M. Navarro-Tapia, C. Camacho-Penalosa, and J. Esteban, "Beam-scanning performance of a slot array antenna on a composite right/left-handed waveguide," in *Proc. 41st Eur. Microwave Conf. (EuMC)*, 2011, pp. 575–578.

[14] M. Navarro-Tapia, J. Esteban, and C. Camacho-Penalosa, "On the actual possibilities of applying the composite right/left-handed waveguide technology to slot array antennas," *IEEE Trans. Antennas Propag.*, vol. 60, pp. 2183–2193, 2012.

[15] D. Yan and W. Ke, "Miniaturization techniques of substrate integrated waveguide circuits," in *Proc. IEEE MTT-S Int. Microwave Workshop Series on Art of Miniaturizing RF and Microwave Passive Components*, 2008, pp. 63–66.

[16] T. Yang, P.-L. Chi, and R.-M. Xu, "Novel composite right/left-handed leaky-wave antennas based on the folded sub-strate-Integrated-Waveguide structures," *Progr. Electromagn. Res. C*, vol. 29, pp. 235–248, 2012.

[17] Q. Yang and Y. Zhang, "Non-radiative composite right/left-handed transmission line based on ridge substrate integrated waveguide," *Electron. Lett.*, vol. 49, pp. 1280–1282, 2013.

[18] *Left-Handed Metamaterial Design Guide*. Norwood, MA, USA: Ansoft Corporation, 2007.